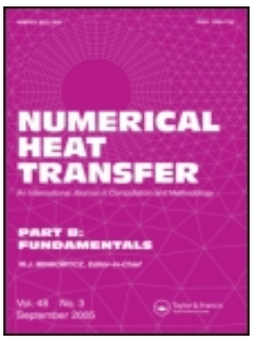

Taylor & Francis
Taylor & Francis Group

Numerical Heat Transfer, Part B: Fundamentals
An International Journal of Computation and Methodology

ISSN: 1040-7790 (Print) 1521-0626 (Online) Journal homepage: http://www.tandfonline.com/loi/unhb20

An improved particle smoothing procedure for Laplacian operator in a randomly scattered cloud

Yao-Hsin Hwang, K. C. Ng & Tony W. H. Sheu

To cite this article: Yao-Hsin Hwang, K. C. Ng & Tony W. H. Sheu (2016) An improved particle smoothing procedure for Laplacian operator in a randomly scattered cloud, Numerical Heat Transfer, Part B: Fundamentals, 70:2, 111-135, DOI: 10.1080/10407790.2016.1177403

To link to this article: http://dx.doi.org/10.1080/10407790.2016.1177403

NUMERICAL HEAT TRANSFER, PART B
2016, VOL. 70, NO. 2, 111–135
http://dx.doi.org/10.1080/10407790.2016.1177403

Taylor & Francis
Taylor & Francis Group

An improved particle smoothing procedure for Laplacian operator in a randomly scattered cloud

Yao-Hsin Hwang[a], K. C. Ng[b], and Tony W. H. Sheu[c]

[a]Department of Marine Engineering, National Kaohsiung Marine University, Cijin District, Kaohsiung, Taiwan; [b]Center of Advanced Computational Engineering, Department of Mechanical Engineering, Universiti Tenaga Nasional, Kajang, Selangor, Malaysia; [c]Department of Engineering Science and Ocean Engineering, National Taiwan University, Taipei, Taiwan

ABSTRACT

In the present study, an improved particle smoothing (IPS) procedure is proposed to imitate the Laplacian operator in a randomly scattered particle cloud. It is devised to provide a more accurate mathematical representation of diffusion term in the moving particle methods. From the numerical analyses, the major source of conventional particle smoothing (PS) schemes leading to solution inaccuracy can be attributed to the intrinsic artificial convection term, whose accuracy order is of $O(\delta^{-1})$. Spatial accuracy can be improved by eliminating the numerically induced artificial velocity in the proposed IPS scheme. Verification studies are performed by testing the proposed scheme in pure diffusion problems. Benchmark lid-driven cavity and backward-facing step flow problems are solved to demonstrate the superiority of the proposed scheme. In the light of numerical analysis and computational results, it is concluded that the proposed IPS scheme is effective to simulate fluid flow problems in the context of moving particle methods.

ARTICLE HISTORY
Received 14 October 2015
Accepted 11 March 2016

1. Introduction

Since the pioneering simulation works of Lucy [1] and Gingold and Monaghan [2] in astrophysics and thanks to vast developments in the past decade, the particle method is a versatile tool to predict intricate engineering problems with complicated geometries ranging from free-surface flow, interfacial flow, and flow structure interaction phenomena [3–6]. Compared with the widely used grid-based routines, simulation can be proceeded without a priori knowledge of topological connection among computational particles. Computationally elaborate procedure to establish a suitable mesh to cope with complicated boundaries can be, therefore, completely avoided. In addition, the problem for flow convection term which must be well handled in grid-based methods to avoid solution inaccuracy/oscillation can be entirely circumvented with the simple particle-moving strategy [7–9]. Owing to the lack of computational particle connection topology, it is, however, computationally challenging to provide an accurate representation of flow diffusion term (Laplacian operator) with a randomly scattered particle distribution. In a conventional particle method, the Laplacian operator is generally imitated through a particle summation procedure [10–12]. While only quite a simple manipulation is demanded, its accuracy can be deteriorated unless in a regular particle arrangement which is generally not encountered in a practical engineering problem. In fact, there are many numerical evidences in the literature showing that the results cannot be accurately calculated without a refined particle

CONTACT Yao-Hsin Hwang yhhwang@webmail.nkmu.edu.tw Department of Marine Engineering, National Kaohsiung Marine University, No. 482, Jhong Jhou 3rd Road, Cijin District, Kaohsiung 805, Taiwan.
Color version of one or more of the figures in this article can be found online at www.tandfonline.com/unhb.

distribution [13–15]. Therefore, proposals addressing on how to accurately approximate the Laplacian operator in an irregular particle distribution become essential, while applying moving particle methods [16–18].

It has been well known that the convection term instead of the diffusion term plays the dominant role in practical engineering problems involving consequential fluid flow motion. Meanwhile, the diffusion process will physically smear rather than reinforce or preserve spatial variation of the solution. This may explain why a simple particle summation procedure can still provide convincing simulations in certain flow problems. It is therefore an act of wisdom not to invest massive computational resource in pursuit of highly accurate discretized diffusion portrayals [19]. In this light, our goal of the present work is to seek a practical modification to improve the conventional particle summation procedure for the diffusion operator. With this goal in mind, the present study is designed to explore the numerical quintessence of the particle smoothing (PS) procedure for the Laplacian operator in the moving particle semi-implicit (MPS) method [11,20]. Also, we aim to provide a practical improvement to yield a more accurate simulation. Numerical analyses will be performed to unveil the computational deficiency inherited by the original PS formulation: adoption of a more compact particle distribution may not yield a better representation of the results. It is manifested that the formal accuracy order of the PS scheme is $O(\delta^{-1})$ with δ being the characteristic particle spacing. This deficiency results from the consequence of the numerically induced convection term. To amend this disadvantage, a simple but effective modification based on the numerical analyses is proposed to eliminate the contaminating terms with $O(\delta^{-1})$. Although it will not result in an unconditionally consistent expression, the formal order of accuracy can be raised to $O(1)$ without the artificial convection term. Numerical validations are performed in one-, two-, and three-dimensional cases to demonstrate the effectiveness of the proposed improved particle smoothing (IPS) strategy. Essential artificial velocity and effective diffusivity of the numerical schemes resulting from an irregular particle distribution are recognized. These parameters are crucial for improving the effectiveness of numerical schemes and they can be used as meaningful indicators for measuring the particle distribution quality. Classic benchmark lid-driven cavity and backward-facing step flow problems are solved to verify the feasibility of the proposed scheme. The present formulation will be shown to be a practical tool in simulating fluid flow motion in the context of moving particle methods.

The content of this paper is organized as follows. The particle smoothing procedure in a conventional moving particle method is described and analyzed in Section 2. This section introduces the particle summation procedure to yield more concise expressions for particle-related operators. Section 3 details the new particle smoothing strategy designed to enhance the accuracy of the discretized Laplacian operator. Numerical validations on the one-, two-, and three-dimensional conduction and two practical flow problems are performed in Section 4. Finally, Section 5 is devoted to the conclusive remarks drawn from the present work.

2. Original particle smoothing scheme

The original particle smoothing (PS) procedure of Zhang et al. [20] for the approximation of gradient and Laplacian operators affixed to the i-th particle can be read as:

$$\langle \nabla \phi \rangle_{PS} = \frac{d}{\sum_{j \neq i} \omega(|\vec{r}_j - \vec{r}_i|, r_e)} \sum_{j \neq i} \frac{(\phi_j - \phi_i)(\vec{r}_j - \vec{r}_i)\omega(|\vec{r}_j - \vec{r}_i|, r_e)}{|\vec{r}_j - \vec{r}_i|^2} \tag{1}$$

$$\langle \nabla^2 \phi \rangle_{PS} = \frac{2d}{\sum_{j \neq i} \omega(|\vec{r}_j - \vec{r}_i|, r_e)} \sum_{j \neq i} \frac{(\phi_j - \phi_i)\omega(|\vec{r}_j - \vec{r}_i|, r_e)}{|\vec{r}_j - \vec{r}_i|^2}. \tag{2}$$

In the above expressions, d is the spatial dimension and $\omega(r \equiv |\vec{r}_j - \vec{r}_i|, r_e)$ denotes the preassigned weighting function defined as:

$$\omega(r, r_e) = \max\left(\frac{r_e}{r} - 1, 0\right). \tag{3}$$

Note that the cutoff radius is chosen as $r_e = 2\delta$ in the present work. In the above three equations, $\vec{r}$ is the position vector and δ is the characteristic particle spacing. It is noted that these operators are derived statistically within the context of isotropic uniform particle distribution, leading to the accuracy order of $O(\delta^2)$. Nevertheless, second-order accuracy is hardly satisfied in a practical scattered particle cloud.

To analyze the PS model and propose our improved version, derivation details are given here for the two-dimensional case ($d = 2$) for the sake of conciseness and comprehension. In the same vein, both one- and three-dimensional situations ($d = 1$ and 3) can be similarly derived. First, we define the following summation operators,

$$\Phi_p^{(q,r)} = \sum_{j \neq i} \frac{(\phi_j - \phi_i)(x_j - x_i)^q (y_j - y_i)^r \omega(|\vec{r}_j - \vec{r}_i|, r_e)}{|\vec{r}_j - \vec{r}_i|^p} \tag{4}$$

$$\Omega_p^{(q,r)} = \sum_{j \neq i} \frac{(x_j - x_i)^q (y_j - y_i)^r \omega(|\vec{r}_j - \vec{r}_i|, r_e)}{|\vec{r}_j - \vec{r}_i|^p}, \tag{5}$$

where the particle position vector is expressed by $\vec{r} = x\vec{i} + y\vec{j}$ and $|\vec{r}| = \sqrt{x^2 + y^2}$. It is worth noting that the summation operator, $\Omega_p^{(q,r)}$, is only affected by the particle distribution and is independent of the solution values. Once the particle distribution has been determined, its value can be straightforwardly obtained. Meanwhile, its order of magnitude expressed in terms of particle spacing is:

$$O(\Omega_p^{(q,r)}) = O(\delta^{q+r-p}) \tag{6}$$

since $O(x_j - x_i) = O(y_j - y_i) = O(|\vec{r}_j - \vec{r}_i|) = O(\delta)$. Therefore, the original PS model for the Laplacian operator in Eq. (2) can then be more compactly rewritten by the following form:

$$\langle \nabla^2 \phi \rangle_{PS} = \frac{4\phi_2^{(0,0)}}{\Omega_0^{(0,0)}}. \tag{7}$$

Performing the Taylor series expansion of ϕ_j with respect to φ_i at the location (x_i, y_i) yields,

$$\phi_j - \phi_i = \phi_x(x_j - x_i) + \phi_y(y_j - y_i) + \frac{1}{2}\phi_{xx}(x_j - x_i)^2 + \phi_{xy}(x_j - x_i)(y_j - y_i) + \frac{1}{2}\phi_{yy}(y_j - y_i)^2 + O(\delta^3), \tag{8}$$

where ϕ_x denotes the partial derivative of the solution variable with respect to x. By substituting this expression into Eq. (4), we can get the following relation by virtue of Eq. (5):

$$\Phi_p^{(q,r)} = \Omega_p^{(q+1,r)}\phi_x + \Omega_p^{(q,r+1)}\phi_y + \frac{1}{2}\Omega_p^{(q+2,r)}\phi_{xx} + \Omega_p^{(q+1,r+1)}\phi_{xy} + \frac{1}{2}\Omega_p^{(q,r+2)}\phi_{yy} + O(\delta^{q+r+3-p}). \tag{9}$$

As a result, the original particle smoothing formulation described in Eq. (2) or (7) can be recast to the following differential form:

$$\langle \nabla^2 \phi \rangle_{\mathrm{PS}} = \frac{4\Omega_2^{(1,0)}}{\Omega_0^{(0,0)}}\phi_x + \frac{4\Omega_2^{(0,1)}}{\Omega_0^{(0,0)}}\phi_y + \frac{2\Omega_2^{(2,0)}}{\Omega_0^{(0,0)}}\phi_{xx} + \frac{4\Omega_2^{(1,1)}}{\Omega_0^{(0,0)}}\phi_{xy} + \frac{2\Omega_2^{(0,2)}}{\Omega_0^{(0,0)}}\phi_{yy} + O(\delta). \tag{10}$$

It is obvious that the original PS model fails to provide a consistent expression for Laplacian operator (or $\langle \nabla^2\phi\rangle_{\mathrm{PS}} \neq \phi_{xx}+\phi_{yy}$ as $\delta\to 0$) unless

$$\Omega_2^{(1,0)} = \Omega_2^{(0,1)} = \Omega_2^{(1,1)} = 0 \qquad \text{and} \qquad \Omega_2^{(2,0)} = \Omega_2^{(0,2)} = \frac{1}{2}\Omega_0^{(0,0)}. \tag{11}$$

The above two equations are no longer satisfied in a randomly scattered particle cloud. On the contrary, its accuracy order becomes $O(\delta^{-1})$ if

$$\Omega_2^{(1,0)} \neq 0 \quad \text{or} \quad \Omega_2^{(0,1)} \neq 0. \tag{12}$$

Equation (12) is a common consequence in physical domain with arbitrarily distributed particles. Thanking to this simple analysis, we are rendered to know the reason why simulation accuracy cannot be ameliorated by refining the particle distribution. Further examination of the equivalent Eq. (10) reveals that the two leading error terms $\frac{4\Omega_2^{(1,0)}}{\Omega_0^{(0,0)}}\phi_x$ and $\frac{4\Omega_2^{(0,1)}}{\Omega_0^{(0,0)}}\phi_y$ can be inferred as the numerically induced artificial convection terms stemming from an inappropriate discretization. The induced artificial velocity components in the x and y directions are as follows:

$$u_N = \frac{4\Omega_2^{(1,0)}}{\Omega_0^{(0,0)}} \qquad \text{and} \qquad v_N = \frac{4\Omega_2^{(0,1)}}{\Omega_0^{(0,0)}}. \tag{13}$$

It is apparent that the terms u_N and v_N are crucially affected by the computational particle distribution, implying that these parameters can be used as the underlying indicators for measuring the particle distribution quality. A suitable particle distribution can be considered to be the one with smaller artificial velocity. Accordingly, these artificial velocity components can be numerically realized by practicing the operations on specific functions:

$$u_N = \left\langle \nabla^2(x)\right\rangle_{\mathrm{PS}} \quad \text{and} \quad v_N = \left\langle \nabla^2(y)\right\rangle_{\mathrm{PS}}. \tag{14}$$

3. Improved particle smoothing scheme

3.1. New formulation on IPS

From the numerical analysis on the PS scheme [20], it is a natural attempt to put forward a modification so as to increase the discretization accuracy by eradicating the leading artificial convection terms:

$$\left\langle \nabla^2\phi\right\rangle_{\mathrm{IPS}} = \left\langle \nabla^2\phi\right\rangle_{\mathrm{PS}} - \frac{4\Omega_2^{(1,0)}}{\Omega_0^{(0,0)}}\langle\phi_x\rangle - \frac{4\Omega_2^{(0,1)}}{\Omega_0^{(0,0)}}\left\langle\phi_y\right\rangle = \frac{4}{\Omega_0^{(0,0)}}\left[\phi_2^{(0,0)} - \Omega_2^{(1,0)}\langle\phi_x\rangle - \Omega_2^{(0,1)}\left\langle\phi_y\right\rangle\right]. \tag{15}$$

As shown in the above equation, the solution gradient terms $\langle\phi_x\rangle$ and $\langle\phi_y\rangle$ must be appropriately realized to have the discretization accuracy of $O(\delta)$ at least.

To provide an accurate representation of the gradient operator, we resort to the original formulation of the gradient model given in Eq. (1), which can be rearranged as:

$$\langle\phi_x\rangle_{\mathrm{PS}} = \frac{2\Phi_2^{(1,0)}}{\Omega_0^{(0,0)}} \qquad \text{and} \qquad \left\langle\phi_y\right\rangle_{\mathrm{PS}} = \frac{2\Phi_2^{(0,1)}}{\Omega_0^{(0,0)}}. \tag{16}$$

According to the Taylor series expansions for the expressions of $\Phi_2^{(1,0)}$ and $\Phi_2^{(0,1)}$,

$$\phi_2^{(1,0)} = \Omega_2^{(2,0)}\phi_x + \Omega_2^{(1,1)}\phi_y + O(\delta) \tag{17a}$$

$$\Phi_2^{(0,1)} = \Omega_2^{(1,1)}\phi_x + \Omega_2^{(0,2)}\phi_y + O(\delta), \tag{17a}$$

the gradient operators with $O(\delta)$ accuracy can be asserted by the following system of equations:

$$\Phi_2^{(1,0)} = \Omega_2^{(2,0)}\langle\phi_x\rangle + \Omega_2^{(1,1)}\left\langle\phi_y\right\rangle \tag{18a}$$

$$\Phi_2^{(0,1)} = \Omega_2^{(1,1)}\langle\phi_x\rangle + \Omega_2^{(0,2)}\left\langle\phi_y\right\rangle, \tag{18b}$$

or expressed explicitly by its equivalent form given below:

$$\langle\phi_x\rangle = \frac{\Omega_2^{(0,2)}\Phi_2^{(1,0)} - \Omega_2^{(1,1)}\Phi_2^{(0,1)}}{\Omega_2^{(2,0)}\Omega_2^{(0,2)} - \left(\Omega_2^{(1,1)}\right)^2} \tag{19a}$$

$$\left\langle\phi_y\right\rangle = \frac{-\Omega_2^{(1,1)}\Phi_2^{(1,0)} + \Omega_2^{(2,0)}\Phi_2^{(0,1)}}{\Omega_2^{(2,0)}\Omega_2^{(0,2)} - \left(\Omega_2^{(1,1)}\right)^2}, \tag{19b}$$

It is noted that the direct employment of Eq. (16) for solution gradient will result in $O(1)$ accuracy of φ_x and φ_y. Substitution of Eq. (18) or (19) into Eq. (15) leads to the modified expression for the differenced Laplacian operator:

$$\left\langle\nabla^2\phi\right\rangle_{\mathrm{IPS}} = \frac{4}{\Omega_0^{(0,0)}}\left[\Phi_2^{(0,0)} - \frac{\Omega_2^{(1,0)}\Omega_2^{(0,2)} - \Omega_2^{(0,1)}\Omega_2^{(1,1)}}{\Omega_2^{(2,0)}\Omega_2^{(0,2)} - \left(\Omega_2^{(1,1)}\right)^2}\Phi_2^{(1,0)} - \frac{\Omega_2^{(0,1)}\Omega_2^{(2,0)} - \Omega_2^{(1,0)}\Omega_2^{(1,1)}}{\Omega_2^{(2,0)}\Omega_2^{(0,2)} - \left(\Omega_2^{(1,1)}\right)^2}\Phi_2^{(0,1)}\right]. \tag{20}$$

Arithmetically, nine summation operators and one 2×2 matrix inversion procedure must be manipulated in this model. Note that only two summation operators ($\Omega_0^{(0,0)}$ and $\Phi_2^{(0,0)}$) are required in the original PS procedure.

3.2. Analysis of the new IPS formulation

The associated modified differential operator for the IPS scheme can be derived as follows by the Taylor series analysis:

$$\begin{aligned}\left\langle\nabla^2\phi\right\rangle_{\mathrm{IPS}} =& \frac{2}{\Omega_0^{(0,0)}}\left[\Omega_2^{(2,0)} - \frac{\Omega_2^{(1,0)}\Omega_2^{(0,2)} - \Omega_2^{(0,1)}\Omega_2^{(1,1)}}{\Omega_2^{(2,0)}\Omega_2^{(0,2)} - \left(\Omega_2^{(1,1)}\right)^2}\Omega_2^{(3,0)} - \frac{\Omega_2^{(0,1)}\Omega_2^{(2,0)} - \Omega_2^{(1,0)}\Omega_2^{(1,1)}}{\Omega_2^{(2,0)}\Omega_2^{(0,2)} - \left(\Omega_2^{(1,1)}\right)^2}\Omega_2^{(2,1)}\right]\phi_{xx} \\ &+ \frac{4}{\Omega_0^{(0,0)}}\left[\Omega_2^{(1,1)} - \frac{\Omega_2^{(1,0)}\Omega_2^{(0,2)} - \Omega_2^{(0,1)}\Omega_2^{(1,1)}}{\Omega_2^{(2,0)}\Omega_2^{(0,2)} - \left(\Omega_2^{(1,1)}\right)^2}\Omega_2^{(2,1)} - \frac{\Omega_2^{(0,1)}\Omega_2^{(2,0)} - \Omega_2^{(1,0)}\Omega_2^{(1,1)}}{\Omega_2^{(2,0)}\Omega_2^{(0,2)} - \left(\Omega_2^{(1,1)}\right)^2}\Omega_2^{(1,2)}\right]\phi_{xy} \\ &+ \frac{2}{\Omega_0^{(0,0)}}\left[\Omega_2^{(0,2)} - \frac{\Omega_2^{(1,0)}\Omega_2^{(0,2)} - \Omega_2^{(0,1)}\Omega_2^{(1,1)}}{\Omega_2^{(2,0)}\Omega_2^{(0,2)} - \left(\Omega_2^{(1,1)}\right)^2}\Omega_2^{(1,2)} - \frac{\Omega_2^{(0,1)}\Omega_2^{(2,0)} - \Omega_2^{(1,0)}\Omega_2^{(1,1)}}{\Omega_2^{(2,0)}\Omega_2^{(0,2)} - \left(\Omega_2^{(1,1)}\right)^2}\Omega_2^{(0,3)}\right]\phi_{yy} + O(\delta).\end{aligned} \tag{21}$$

While the new formulation still remains to be conditionally consistent, the artificial convection term with $O(\delta^{-1})$ has been effectively eliminated. The effective diffusivity tensor in association with this modification can then be obtained as:

$$\tau_{xx} = \frac{2}{\Omega_0^{(0,0)}}\left[\Omega_2^{(2,0)} - \frac{\Omega_2^{(1,0)}\Omega_2^{(0,2)} - \Omega_2^{(0,1)}\Omega_2^{(1,1)}}{\Omega_2^{(2,0)}\Omega_2^{(0,2)} - \left(\Omega_2^{(1,1)}\right)^2}\Omega_2^{(3,0)} - \frac{\Omega_2^{(0,1)}\Omega_2^{(2,0)} - \Omega_2^{(1,0)}\Omega_2^{(1,1)}}{\Omega_2^{(2,0)}\Omega_2^{(0,2)} - \left(\Omega_2^{(1,1)}\right)^2}\Omega_2^{(2,1)}\right] \tag{22a}$$

$$\tau_{xy} = \frac{2}{\Omega_0^{(0,0)}}\left[\Omega_2^{(1,1)} - \frac{\Omega_2^{(1,0)}\Omega_2^{(0,2)} - \Omega_2^{(0,1)}\Omega_2^{(1,1)}}{\Omega_2^{(2,0)}\Omega_2^{(0,2)} - \left(\Omega_2^{(1,1)}\right)^2}\Omega_2^{(2,1)} - \frac{\Omega_2^{(0,1)}\Omega_2^{(2,0)} - \Omega_2^{(1,0)}\Omega_2^{(1,1)}}{\Omega_2^{(2,0)}\Omega_2^{(0,2)} - \left(\Omega_2^{(1,1)}\right)^2}\Omega_2^{(1,2)}\right] \tag{22b}$$

$$\tau_{yy} = \frac{2}{\Omega_0^{(0,0)}}\left[\Omega_2^{(0,2)} - \frac{\Omega_2^{(1,0)}\Omega_2^{(0,2)} - \Omega_2^{(0,1)}\Omega_2^{(1,1)}}{\Omega_2^{(2,0)}\Omega_2^{(0,2)} - \left(\Omega_2^{(1,1)}\right)^2}\Omega_2^{(1,2)} - \frac{\Omega_2^{(0,1)}\Omega_2^{(2,0)} - \Omega_2^{(1,0)}\Omega_2^{(1,1)}}{\Omega_2^{(2,0)}\Omega_2^{(0,2)} - \left(\Omega_2^{(1,1)}\right)^2}\Omega_2^{(0,3)}\right]. \tag{22c}$$

Like the artificial velocity in the PS scheme, these effective diffusivity components can be utilized as the useful indicators to measure particle distribution quality in the IPS scheme to mimic Laplacian operator. Similarly, these parameters can also be attained by practicing the IPS scheme on specific functions:

$$\tau_{xx} = \left\langle \nabla^2\left(\frac{x^2}{2}\right)\right\rangle_{\text{IPS}},\ \tau_{xy} = \left\langle \nabla^2\left(\frac{xy}{2}\right)\right\rangle_{\text{IPS}} \text{ and } \tau_{yy} = \left\langle \nabla^2\left(\frac{y^2}{2}\right)\right\rangle_{\text{IPS}}. \tag{23}$$

3.3. One- and three-dimensional IPS formulations

Following the same derivation procedures, the IPS models for the one- and three-dimensional Laplacian operators can be derived and they are summarized below:

(a) One-dimensional IPS model:

$$\langle \phi_{xx}\rangle_{\text{IPS}} = \frac{2}{\Omega_0^{(0)}}\left[\Phi_2^{(0)} - \frac{\Omega_2^{(1)}}{\Omega_0^{(0)}}\Phi_2^{(1)}\right], \tag{24}$$

where the one-dimensional summation operators are defined as:

$$\Phi_p^{(q)} = \sum_{j\neq i}\frac{(\phi_j - \phi_i)(x_j - x_i)^q\omega(\left|\vec{r}_j - \vec{r}_i\right|, r_e)}{\left|\vec{r}_j - \vec{r}_i\right|^p} \tag{25a}$$

$$\Omega_p^{(q)} = \sum_{j\neq i}\frac{(x_j - x_i)^q\omega(\left|\vec{r}_j - \vec{r}_i\right|, r_e)}{\left|\vec{r}_j - \vec{r}_i\right|^p}. \tag{25b}$$

(b) Three-dimensional IPS model:

$$\left\langle \nabla^2\phi\right\rangle_{\text{IPS}} = \frac{6}{\Omega_0^{(0,0,0)}}\left[\Phi_2^{(0,0,0)} - \Omega_2^{(1,0,0)}\langle\phi_x\rangle - \Omega_2^{(0,10)}\left\langle\phi_y\right\rangle - \Omega_2^{(0,0,1)}\langle\phi_z\rangle\right] \tag{26}$$

The gradient operators are derived as follows:

$$\Phi_2^{(1,0,0)} = \Omega_2^{(2,0,0)}\langle\phi_x\rangle + \Omega_2^{(1,1,0)}\left\langle\phi_y\right\rangle + \Omega_2^{(1,0,1)}\langle\phi_z\rangle \tag{27a}$$

$$\Phi_2^{(0,1,0)} = \Omega_2^{(1,1,0)}\langle\phi_x\rangle + \Omega_2^{(0,2,0)}\left\langle\phi_y\right\rangle + \Omega_2^{(0,1,1)}\langle\phi_z\rangle \tag{27b}$$

$$\Phi_2^{(0,0,1)} = \Omega_2^{(1,0,1)}\langle\phi_x\rangle + \Omega_2^{(0,1,1)}\left\langle\phi_y\right\rangle + \Omega_2^{(0,0,2)}\langle\phi_z\rangle. \tag{27c}$$

The above equation system possesses a symmetrical coefficient matrix and can be solved by a suitable matrix inversion procedure. Arithmetically, it requires a total number of 14 summation operators and one 3×3 matrix inversion procedure in IPS model. The associated summation operators are defined as:

$$\Phi_p^{(q,r,s)} = \sum_{j\neq i}\frac{(\phi_j - \phi_i)(x_j - x_i)^q(y_j - y_i)^r(z_j - z_i)^s\omega(\left|\vec{r}_j - \vec{r}_i\right|, r_e)}{\left|\vec{r}_j - \vec{r}_i\right|^p} \tag{28a}$$

$$\Omega_p^{(q,r,s)} = \sum_{j \neq i} \frac{(x_j - x_i)^q (y_j - y_i)^r (z_j - z_i)^s \omega(|\vec{r}_j - \vec{r}_i|, r_e)}{|\vec{r}_j - \vec{r}_i|^p}. \tag{28b}$$

4. Numerical verification

The newly proposed IPS scheme will be verified by comparing the predicted second derivatives with exact solutions. Also, the one-, two-, and three-dimensional pure diffusion problems subjected to boundary conditions are investigated as well. Results will be compared with those obtained from the original PS scheme and the available exact solutions. The introduced artificial velocity and effective diffusivity will be depicted to address the improved discretization accuracy using the IPS numerical scheme. Effects of numerical parameters such as the particle spacing and the distribution irregularity on solution accuracy are also investigated. Finally, the cases of lid-driven cavity flow and flow over a backward-facing step are simulated to show the effectiveness of the present new IPS model.

4.1. One-dimensional case

First, the Laplacian of a given quadratic profile is studied:

$$\phi(x) = \phi_i + a(x - x_i) + b(x - x_i)^2, \tag{29a}$$

where the exact solution of $\langle \phi_{xx} \rangle$ at $x = x_i$ is:

$$\langle \phi_{xx} \rangle_{ex} = 2b. \tag{29b}$$

The discretized operators predicted by PS and IPS can be, respectively, derived as:

$$\langle \phi_{xx} \rangle_{\mathrm{PS}} = 2a \frac{\Omega_2^{(1)}}{\Omega_0^{(0)}} + 2b \tag{30a}$$

$$\langle \phi_{xx} \rangle_{\mathrm{IPS}} = 2b \left[1 - \frac{\Omega_2^{(1)} \Omega_2^{(3)}}{\left(\Omega_0^{(0)}\right)^2} \right]. \tag{30b}$$

Apparently, the PS scheme yields a nonvanished Laplacian under even in a linear field ($b = 0$) which can be attributed to the artificial convection term. The IPS scheme is equipped with an effective diffusivity term $\left(1 - \frac{\Omega_2^{(1)} \Omega_2^{(3)}}{\left(\Omega_0^{(0)}\right)^2}\right)$. These phenomena are consistent with the previous accuracy analyses.

The second test involves the solutions at three points $x = 0$, 1, and $-1 + \alpha$

$$\phi(0) = 0, \quad \phi(1) = 1, \quad \text{and} \quad \phi(-1 + \alpha) = \phi^* \tag{31a}$$

In this problem, α measures the degree of grid nonuniformity (irregularity). In uniform grids, $\alpha = 0$. The exact solution profile satisfying these nodal constraints can be easily derived as:

$$\phi(x) = \frac{(1 - \alpha)^2 - \phi^*}{(1 - \alpha)(2 - \alpha)} x + \frac{1 - \alpha + \phi^*}{(1 - \alpha)(2 - \alpha)} x^2. \tag{31b}$$

Accordingly, the exact Laplacian at $x = 0$ reads:

$$\langle \phi_{xx} \rangle_{\mathrm{ex}} = 2 \frac{1 - \alpha + \phi^*}{(1 - \alpha)(2 - \alpha)}. \tag{31c}$$

The difference approximations can be, respectively, derived in the following for the respective PS and IPS models:

$$\langle \phi_{xx} \rangle_{\mathrm{PS}} = 2\frac{(1-\alpha)^2 + \phi^* \omega^*}{(1-\alpha)^2(1+\omega^*)} \tag{32a}$$

$$\langle \phi_{xx} \rangle_{\mathrm{IPS}} = 2\frac{1-\alpha+\phi^*}{(1-\alpha)(2-\alpha)}\left\{1 - \frac{(1-\alpha-\omega^*)[1-(1-\alpha)\omega^*)]}{(1-\alpha)(1+\omega^*)^2}\right\}. \tag{32b}$$

In the above, ω^* denotes the weighting function for the point at $x = -1+\alpha$:

$$\omega^* = \frac{1+\alpha}{1-\alpha}. \tag{32c}$$

Comparison of exact solution with those obtained by PS and IPS is displayed in Figure 1(*a*) with $\phi^* = 2.0,\ 0.5,\ -0.5$, and -2.0. As evidently shown in this figure, the PS scheme shows a marked discrepancy, especially in the case of nonuniform grid setting. As expected, the IPS scheme has significantly increased the accuracy of the Laplacian operator. To make a closer observation on the effects of grid irregularity, we expand the reality factor of the estimated Laplacians ($z = \langle \phi_{xx} \rangle / \langle \phi_{xx} \rangle_{ex}$) in terms of the grid nonuniformity factor, thereby leading to:

$$\frac{\langle \phi_{xx} \rangle_{\mathrm{PS}}}{\langle \phi_{xx} \rangle_{\mathrm{ex}}} = 1 + \frac{3(\phi^*-1)}{2(\phi^*+1)}\alpha + \frac{(1+9\phi^*+2\phi^{*2})}{2(\phi^*+1)^2}\alpha^2 + O(\alpha^3), \tag{33a}$$

$$\frac{\langle \phi_{xx} \rangle_{\mathrm{IPS}}}{\langle \phi_{xx} \rangle_{\mathrm{ex}}} = 1 - \frac{3}{4}\alpha^2 + \frac{1}{4}\alpha^3. \tag{33b}$$

It is noted that the reality factor in the IPS model is not affected by the solution value (ϕ^*) but is dependent only on the grid nonuniformity factor. This observation is not surprising at all since the reality factor is related to the effective diffusivity in the proposed IPS scheme. Figure 1(*b*) illustrates the resulting reality factor accompanied with an estimated value for PS scheme. This estimated value is obtained by omitting the higher-order terms of the expansion series in Eq. (33a). It is shown that the proposed IPS scheme is comparatively less sensitive to the grid irregularity than the PS scheme. Consequently, the accuracy of the difference Laplacian operator can be effectively brightened up with the proposed IPS scheme.

The third test problem considered in the one-dimensional case is designed to evaluate the difference Laplacian operator with the following solution distribution:

$$\phi(x) = \sin(2\pi x). \tag{34a}$$

A direct differential manipulation on the above solution profile yields the exact Laplacian given by:

$$\nabla^2 \phi_{\mathrm{ex}}(x) = -(2\pi)^2 \sin(2\pi x). \tag{34b}$$

Except at the end points, the interior nodes are randomly assigned to yield an uneven distribution:

$$x_i = (i-1)\Delta x + \alpha(\chi_i - 0.5)\Delta x, \quad i = 2, 3, .., n_C, \tag{35}$$

where n_C is related to the total number of particles, $\Delta x = 1/n_C$ is the characteristic particle spacing (or particle number density), α is the grid irregularity factor, and χ_i is the uniform random number lying between 0 and 1. Laplacian operator is evaluated at these grid nodes with the solution distribution given in Eq. (34a). Figure 2(*a*) elucidates the resulting distributions of normalized Laplacian operator for $n_C = 8$ and 16 with $\alpha = 0.3$. It is shown that the PS scheme predicts viciously oscillatory results with denser particle distribution ($n_C = 16$). On the other hand, the accuracy of the proposed IPS scheme is not deteriorated when denser particle distribution is used. In fact, the corresponding

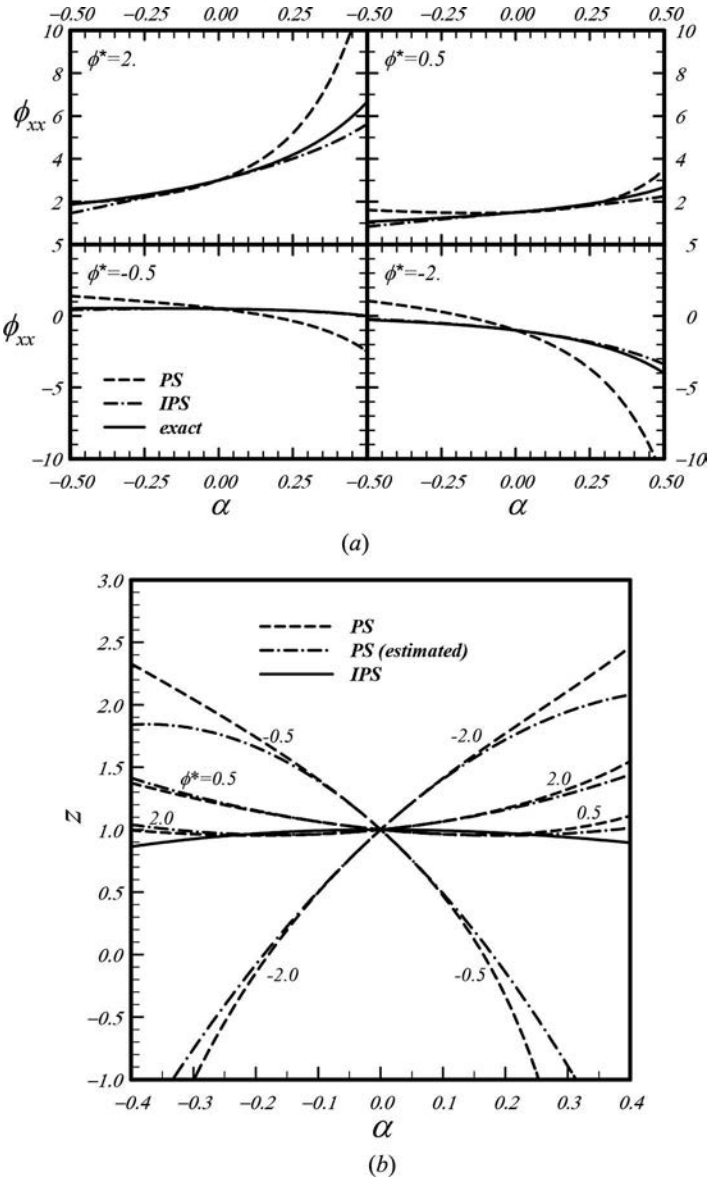

Figure 1. Results of the three-point problem. (*a*) Difference Laplacian at $x = 0$ and (*b*) reality factor of the difference Laplacian operator.

differential operator modeled by the PS scheme can be estimated as:

$$\langle \phi_{xx} \rangle_{\mathrm{PS}^*} = \frac{2\Omega_2^{(1)}}{\Omega_0^{(0)}} \phi_x + \phi_{xx}. \tag{36}$$

Figure 2(*b*) which details on the comparison of this estimation with that provided by PS has successfully verified our previous analysis on the numerical scheme. The Laplacian with PS is overwhelmingly erroneous predicted by the artificial convection term.

The resulting artificial velocity stemming from the PS scheme for the adopted particle number (n_C) with the grid irregularity factors $\alpha = 0.1$, 0.3, and 0.5 is depicted in Figure 3(*a*). This quantity is cast in

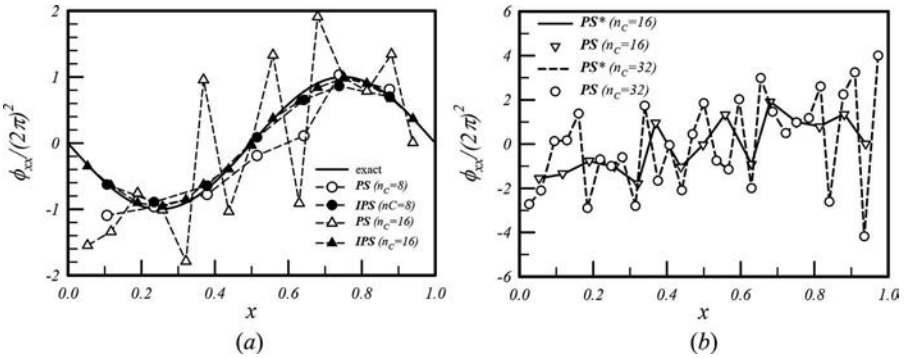

Figure 2. Results of the one-dimensional test problem. (*a*) Distribution of the Laplacian operator and (*b*) reality of the Laplacian operator predicted by PS.

its L2-norm measure:

$$V_N = 2\left\|\frac{\Omega_2^{(1)}}{\Omega_0^{(0)}}\right\|_2. \tag{37a}$$

From this figure, it is evidently observed that the artificial velocity increases with the adopted particle number and grid irregularity as well. It implies that the accuracy of PS scheme cannot be improved by refining the particle spacing. On the contrary, its accuracy will be significantly reduced by the overwhelming artificial velocity. Based on the artificial velocity, we can further introduce an artificial cell Reynolds number to signify the scheme performance:

$$\mathrm{Re}_\delta = V_N\delta = V_N/n_C, \tag{37b}$$

which is illustrated in Figure 3(*b*). As expected, the artificial cell Reynolds number is insensitive to the adopted particle spacing and is only affected by the grid irregularity. Since the artificial cell Reynolds number is independent of the solution distribution, the relative artificial convection term for a sinusoidal profile of $\sin(kx)$ can be estimated as $\mathrm{Re}_\delta\, n_C/k$. Therefore, it is speculated that the physical diffusion term will be exceedingly overwhelmed by the artificial convection term in the cases of low-wavenumber solution and dense particle spacing. As for the IPS scheme, the artificial convection term has been completely eliminated; however, the use of IPS would translate into the appearance of effective diffusivity which can be derived from Eq. (24) as $\tau_{\mathrm{eff}} = 1 - \frac{\Omega_2^{(1)}\Omega_2^{(3)}}{(\Omega_0^{(0)})^2}$. Figure 4 exhibits

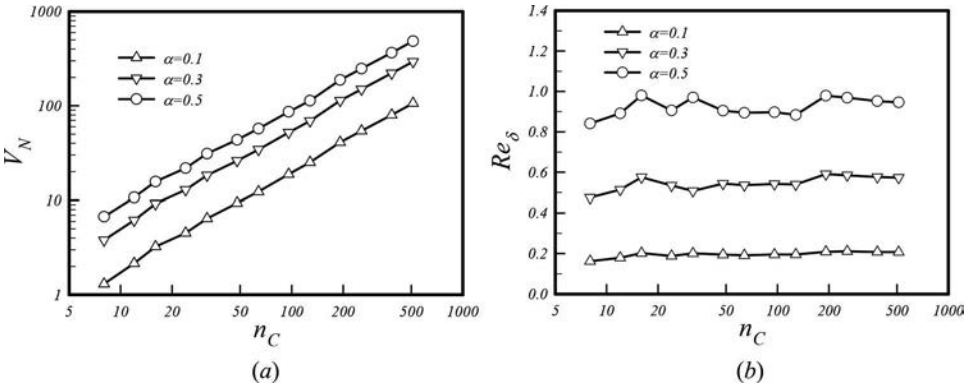

Figure 3. Artificial velocity and cell Reynolds number of PS. (*a*) Artificial velocity and (*b*) artificial cell Reynolds number.

the distribution of the resulting effective diffusivity. Although its accuracy seems to be insensitive to the adopted particle number, the discrepancy between the exact and difference Laplacians is less than 4% in the mildly irregular grid distribution case ($\alpha \leq 0.5$). As compared with the PS scheme, IPS will be a proper alternative to solve the practical engineering problems.

In addition to the numerically induced velocity or diffusivity, error of the difference operator is also assessed by the following L2-norm measure:

$$\varepsilon_m = \left\| \langle \phi_{xx} \rangle_i - \langle \phi_{xx} \rangle_{ex} \right\|_2. \tag{38}$$

Figure 5(*a*) plots the effects of adopted particle spacing on the difference operator error for $\alpha = 0.3$. The results are closely related to the artificial velocity and effective diffusivity for PS and IPS which were shown in Figures 3(*a*) and 4, respectively. The error will be augmented with a refined particle spacing for PS but it is insensitive to the adopted particle number in the case of IPS. Effects of grid irregularity on this error are demonstrated in Figure 5(*b*) with $n_C = 128$. Besides the significant improvement in difference operator accuracy, the IPS scheme is less sensitive to the grid irregularity than PS, owing to the notorious jump in error level (PS scheme) as a slight irregularity is introduced on the regular grid setting ($\alpha = 0$).

Finally, a pure diffusion equation is solved to test the difference Laplacian operator,

$$\frac{\partial \phi}{\partial t} = \frac{\partial^2 \phi}{\partial x^2}. \tag{39a}$$

Computations are performed in the domain of $0 \leq x \leq 1$ and the results are compared with the following exact solution, which is also used to describe the initial and boundary conditions in the current numerical problem:

$$\phi_{\text{ex}}(x, t) = \beta e^{-(2\pi\gamma)^2 t} \sin(2\pi\gamma x) + x. \tag{39b}$$

Simple Euler explicit scheme is used to solve this problem, leading to:

$$\phi_p^{n+1} = \phi_p^n + \Delta t \langle \phi_{xx} \rangle. \tag{39c}$$

The time step is selected as:

$$\Delta t = C_D \frac{\Omega_0^{(0)}}{2\Omega_2^{(0)}}. \tag{39d}$$

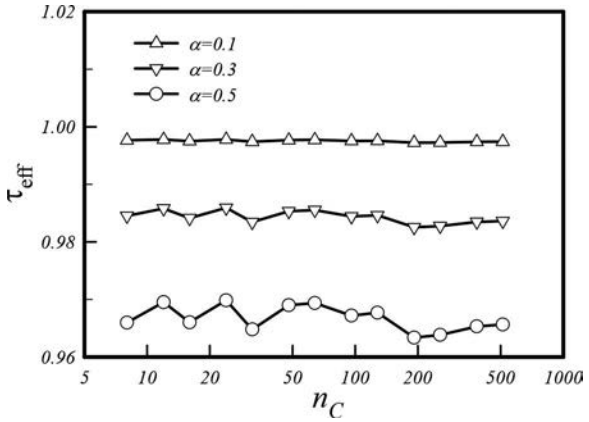

Figure 4. Effective diffusivity of IPS.

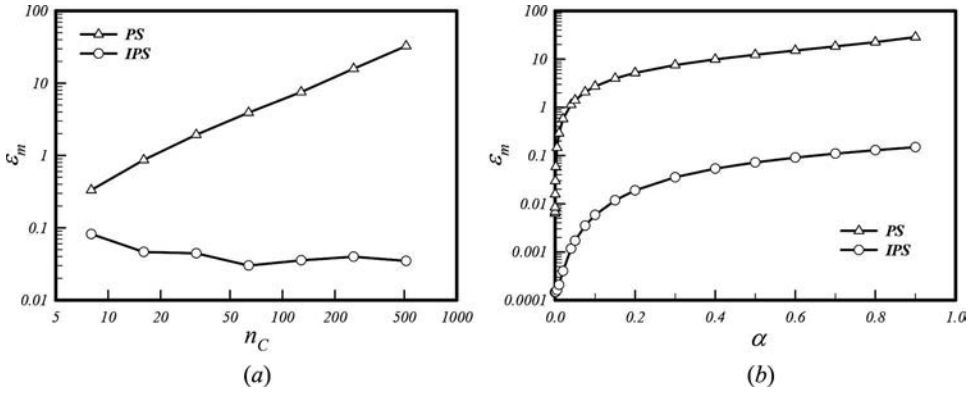

Figure 5. Error in the difference Laplacian operator. (*a*) Effect of the particle spacing (α = 0.3) and (*b*) effect of the grid irregularity ($n_C = 128$).

It is worth noting that a monotone solution can be obtained with $C_D \leq 1$ for PS. Computations are executed under the following set of numerical parameters,

$$n_C = 128, \quad \alpha = 0.3, \quad \beta = 1.0, \quad \gamma = 1.0, \quad \text{and} \quad C_D = 1.0 \tag{39e}$$

The solution distributions obtained by PS at various simulation times for $n_C = 32$, 64, and 128 are plotted in Figure 6(*a*). Interestingly, while it is subjected to a noticeable error of difference Laplacian operator, the PS scheme is able to provide a reasonable result because of the endowed monotone property. It guarantees the nonexistence of unphysical oscillations in the resulting solution. Therefore, the solution accuracy is not deteriorated by refining particle spacing. Comparison with the solution by IPS is elucidated in Figure 6(*b*). It is clearly shown that the proposed IPS scheme is more accurate due to the elimination of artificial convection term appeared in the original PS scheme.

Accuracy of the numerical scheme can be further assessed by investigating the discrepancies between the computational and exact solutions. Similarly, we define a L2-norm solution error measure:

$$\varepsilon_m = \|\phi_i - \phi_{ex}\|_2. \tag{40}$$

Evolutions of the solution error ε_m are demonstrated in Figure 7(*a*)–7(*c*) at different values of n_C, α, and C_D, respectively. As clearly depicted in these figures, the IPS scheme has significantly improved the solution accuracy in all cases. Meanwhile, the adoption of a denser particle spacing does not ensure an increase in solution accuracy, whereas the solution accuracy will be deteriorated by grid irregularity. Furthermore, the resulting solution is insensitive to the adopted time step.

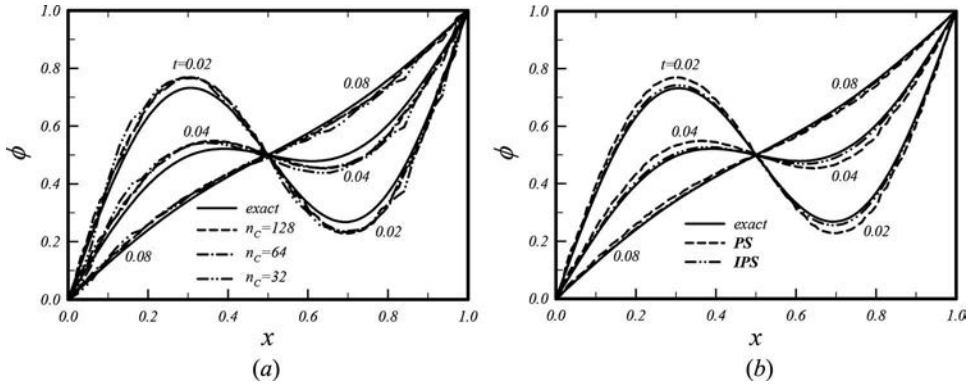

Figure 6. Solution distribution in one-dimensional diffusion problem. (*a*) Predicted solution by PS and (*b*) comparison of the solution profiles predicted by PS and IPS.

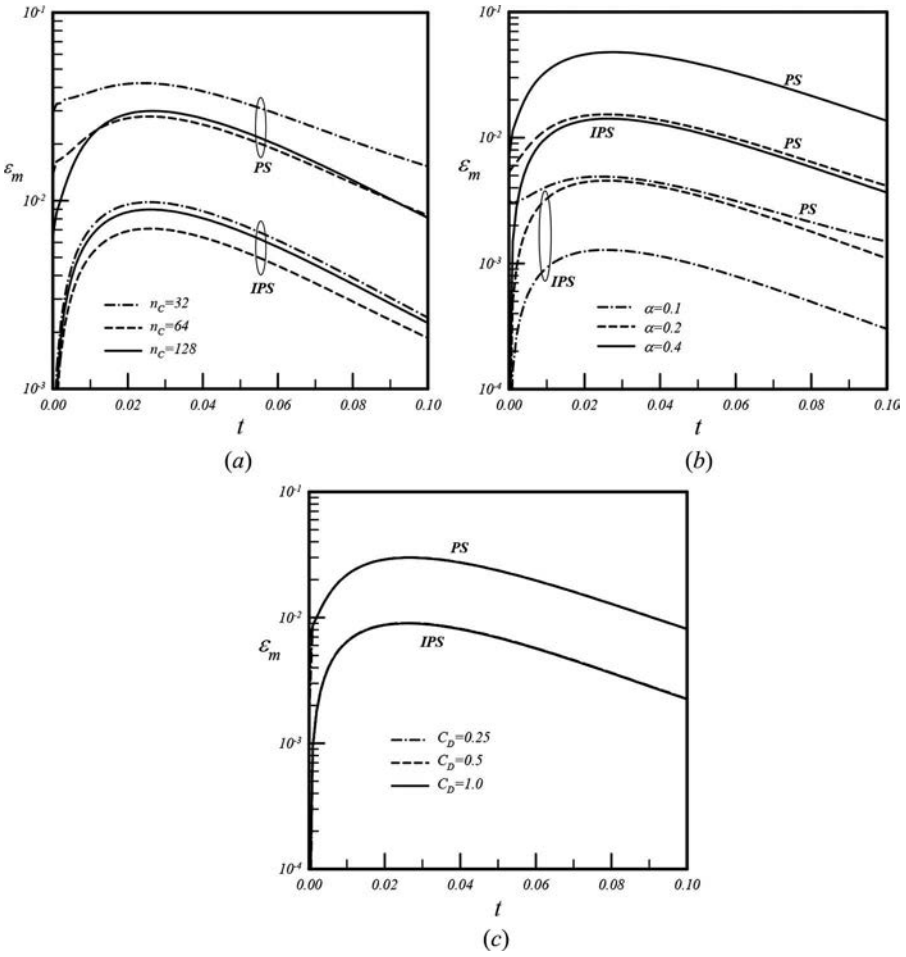

Figure 7. Evolution of the solution error. (*a*) Effect of the particle spacing, (*b*) effect of the grid irregularity, and (c) effect of the time step.

4.2. Two-dimensional case

Similar to the previous one-dimensional case, the particle location is generated by the following relations:

$$x_{ij} = (i-1)\Delta x + \alpha(\chi_{ij}^{(x)} - 0.5)\Delta x, \tag{41a}$$

$$y_{ij} = (j-1)\Delta y + \alpha(\chi_{ij}^{(y)} - 0.5)\Delta y. \tag{41b}$$

In the above, $\Delta x = \Delta y = 1/n_C$ and χ is a random number lying between 0 and 1. With this particle distribution, the artificial velocity (cell Reynolds number) of PS as well as the effective diffusivity of IPS can be directly computed and displayed in Figure 8(*a*)–8(*c*). The artificial cell Reynolds numbers can be written as:

$$\mathrm{Re}_u = u_N/n_C = \frac{4}{n_C}\left\|\frac{\Omega_2^{(1,0)}}{\Omega_0^{(0,0)}}\right\|_2, \tag{42a}$$

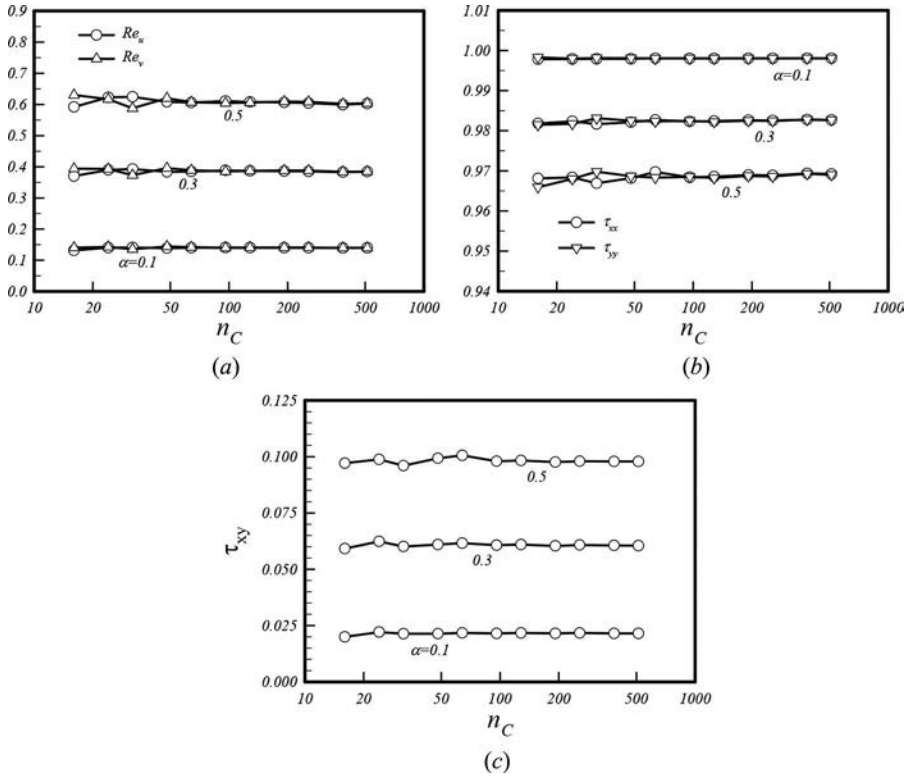

Figure 8. Artificial cell Reynolds number and effective diffusivity of the numerical schemes. (*a*) Artificial cell Reynolds number of PS, (*b*) effective normal diffusivity of IPS, and (*c*) effective shear diffusivity of IPS.

$$\mathrm{Re}_v = v_N/n_C = \frac{4}{n_C}\left\|\frac{\Omega_2^{(0,1)}}{\Omega_0^{(0,0)}}\right\|_2. \tag{42b}$$

In a statistically isotropic particle distribution, the magnitudes of artificial cell Reynolds number and normal diffusivity in x and y direction are nearly the same and are independent of particle number density. Meanwhile, the numerically induced shear diffusivity (τ_{xy}) is mostly responsible for the solution inaccuracy of IPS as compared with its normal parts (τ_{xx} and τ_{yy}).

Difference Laplacian operator is evaluated with the following prescribed distribution:

$$\phi(x,y) = \sin(2\pi x)\sin(2\pi y), \tag{43a}$$

which yields the following exact Laplacian:

$$\nabla^2\phi_{\mathrm{ex}}(x,y) = -2(2\pi)^2\sin(2\pi x)\sin(2\pi y). \tag{43b}$$

For comparison purpose, Eq. (43b) is calculated and the results are plotted in Figure 9. Particle distributions of $\alpha = 0.3$ with $n_C = 8$ and 16 are shown in Figures 10(*a*) and 10(*b*), respectively. Although the deviation from regular distribution can be found in these figures, the particles spread in a rather uniform manner. The corresponding Laplacian predicted by PS for $n_C = 8$ and 16 are illustrated in Figures 11(*a*) and 11(*b*), respectively. Similar to the one-dimensional case, severe oscillation is observed for PS with a denser particle distribution. The predictions of IPS, as expected, are more accurate as shown in Figures 12(*a*) and 12(*b*). Comparison of errors resulting from various Laplacian operators is conducted and the results are exhibited in Figures 13(*a*) and 13(*b*) to signify the effects of particle spacing and grid irregularity, respectively. These results are attributed to the artificial velocity

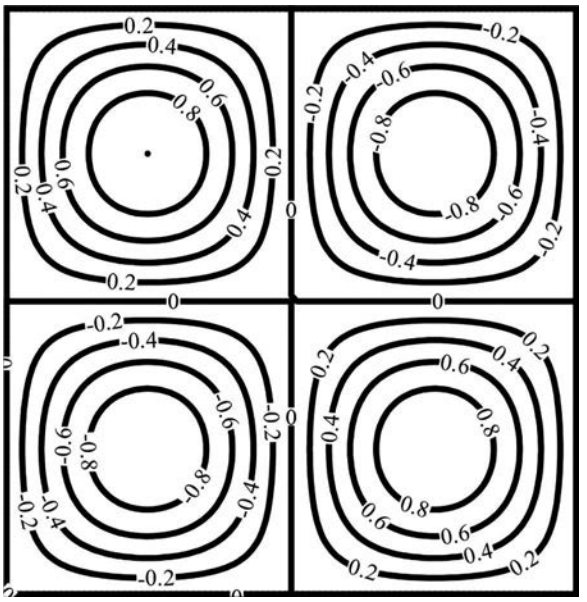

Figure 9. Exact value of the Laplacian operator in the two-dimensional test problem.

and the numerically induced diffusivity given in Figures 8(*a*)–8(*c*). As in the one-dimensional case, the IPS scheme can improve the approximated Laplacian operator and it is less sensitive to grid irregularity.

The following two-dimensional pure diffusion equation is solved:

$$\frac{\partial \phi}{\partial t} = \frac{\partial^2 \phi}{\partial x^2} + \frac{\partial^2 \phi}{\partial y^2}, \tag{44a}$$

and it is amenable to the exact solution given by:

$$\phi_{ex}(x, y, t) = \beta e^{-2(2\pi\gamma)^2 t} \sin(2\pi\gamma x) \sin(2\pi\gamma y) + 4x(x-1) - 4y(y-1) + (x-0.5)(y-0.5). \tag{44b}$$

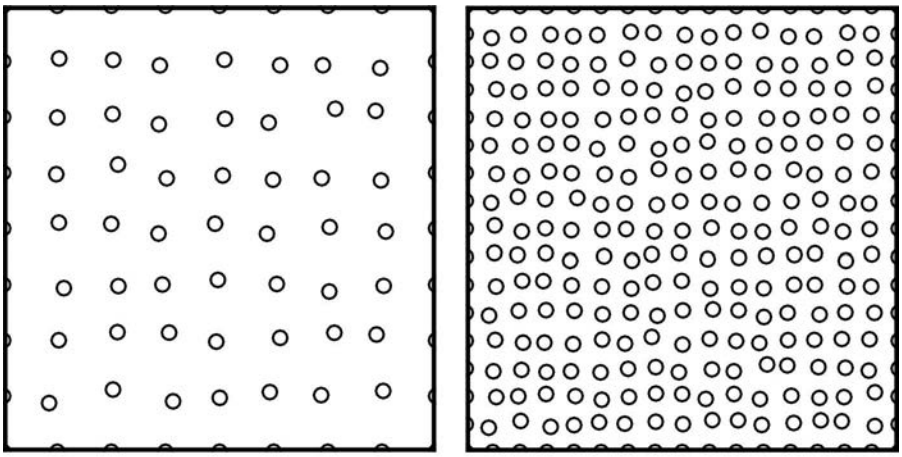

Figure 10. Particle distribution with $\alpha = 0.3$. (*a*) $n_C = 8$ and (*b*) $n_C = 16$.

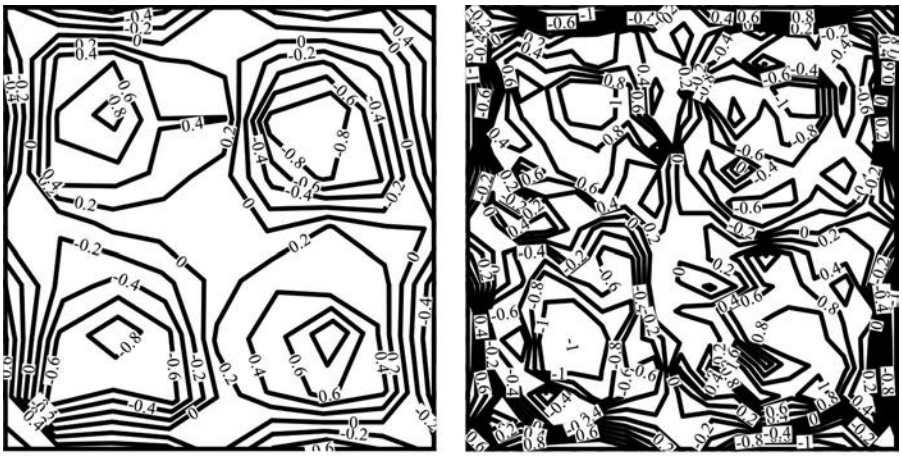

(a) (b)

Figure 11. Laplacian operator value predicted by PS with $\alpha = 0.3$. (*a*) $n_C = 8$ and (*b*) $n_C = 16$.

As in the one-dimensional case, the simple Euler forward scheme is adopted to solve this problem with the time step prescribed as:

$$\Delta t = C_D \frac{\Omega_0^{(0,0)}}{4\Omega_2^{(0,0)}}. \tag{44c}$$

It is worth noting that a monotone solution can be obtained with $C_D \leq 1$ for PS. In our calculations, the following numerical parameters are utilized:

$$n_C = 64, \quad \alpha = 0.3, \quad \beta = 1.0, \quad \gamma = 1.0, \quad \text{and} \quad C_D = 1.0 \tag{44d}$$

The solution errors are plotted in Figure 14(*a*)–14(*c*) to investigate the effects of n_C, α, and C_D, respectively. As clearly shown in these figures, the IPS scheme improves solution accuracy in all cases. Meanwhile, it is seen that the adoption of a denser particle spacing may not necessarily increase the solution accuracy. Solution accuracy will be deteriorated by grid irregularity. The resulting solution is insensitive to the adopted time step. These conclusions are also consistent with those in the

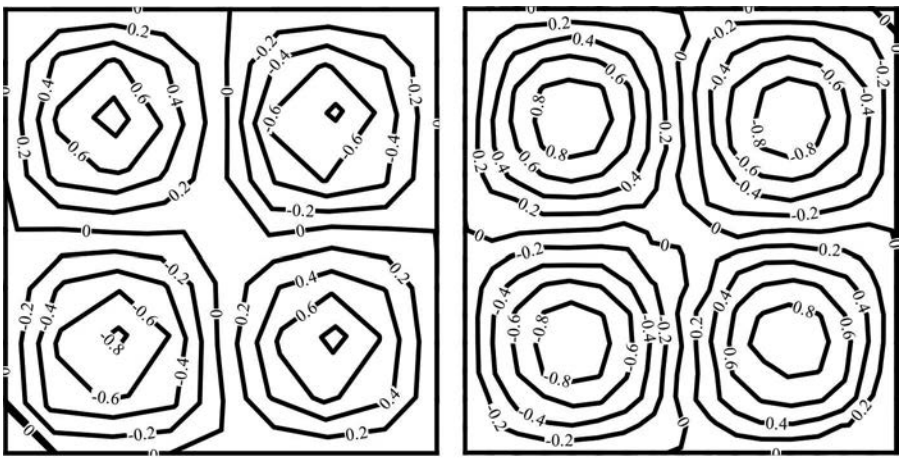

(a) (b)

Figure 12. Laplacian operator value predicted by IPS with $\alpha = 0.3$. (*a*) $n_C = 8$ and (*b*) $n_C = 16$.

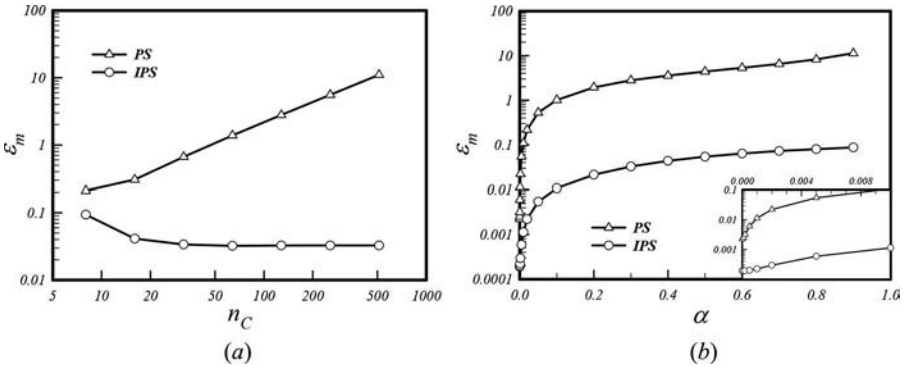

Figure 13. Error of the difference Laplacian operator. (*a*) Effect of the particle spacing ($\alpha = 0.3$) and (*b*) effect of the grid irregularity ($n_C = 128$).

one-dimensional case. Figure 15(*a*)–15(*c*) demonstrates the solution profiles at $t = 0.02$ obtained from the exact, PS and IPS solutions, respectively. Although quite a reasonable result can be obtained by the PS scheme, some unphysical wiggles can be observed in the numerical solution (Figure 15(*b*)).

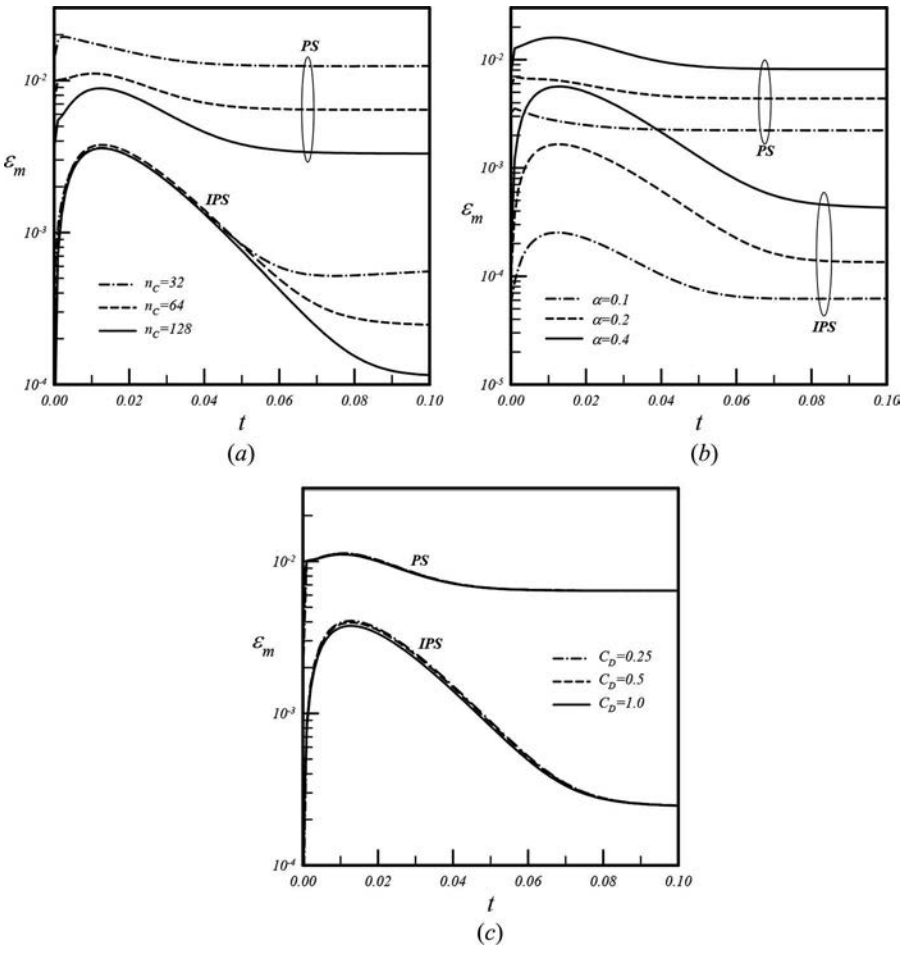

Figure 14. Evolution of the solution error. (*a*) Effect of the particle spacing, (*b*) effect of the grid irregularity, and (*c*) effect of the time step.

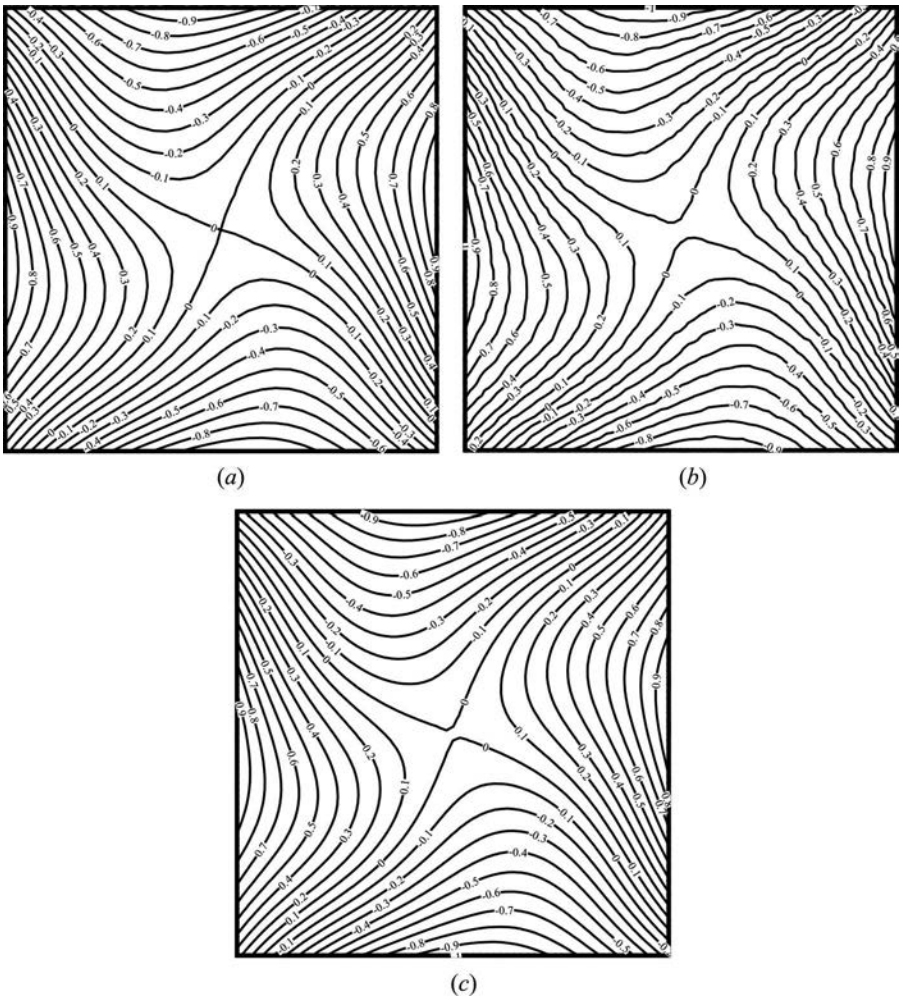

Figure 15. Solution contours computed at $t = 0.02$. (*a*) Exact solution, (*b*) predicted contours by PS, and (*c*) predicted contours by IPS.

4.3. Three-dimensional case

The particle locations in the following three-dimensional analysis are generated by a similar manner as being practiced in the one-dimensional case:

$$x_{ijk} = (i-1)\Delta x + \alpha(\chi_{ijk}^{(x)} - 0.5)\Delta x, \tag{45a}$$

$$y_{ijk} = (j-1)\Delta y + \alpha(\chi_{ijk}^{(y)} - 0.5)\Delta y, \tag{45b}$$

$$z_{ijk} = (k-1)\Delta z + \alpha(\chi_{ijk}^{(z)} - 0.5)\Delta z, \tag{45c}$$

where $\Delta x = \Delta y = \Delta z = 1/n_C$ and χ is the random number with the value lying between 0 and 1. Under this particle distribution, the artificial velocity (cell Reynolds number) of PS and effective diffusivity of IPS can be directly computed and displayed in Figure 16(*a*)–16(*c*). The artificial velocity components can be expressed as:

$$\mathrm{Re}_u = u_N/n_C = \frac{6}{n_C}\left\|\frac{\Omega_2^{(1,0,0)}}{\Omega_0^{(0,0,0)}}\right\|_2, \tag{46a}$$

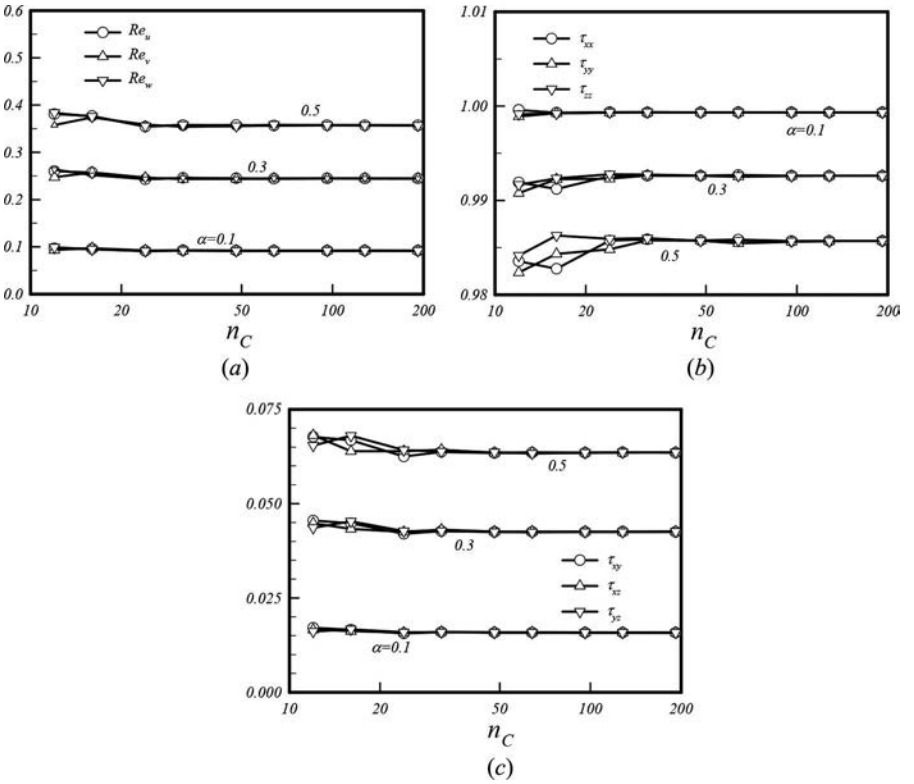

Figure 16. Artificial cell Reynolds number and effective normal diffusivity of the IPS numerical scheme. (*a*) Artificial cell Reynolds number of PS, (*b*) effective normal diffusivity of IPS, and (*c*) effective shear diffusivity of IPS.

$$\mathrm{Re}_v = v_N/n_C = \frac{6}{n_C}\left\|\frac{\Omega_2^{(0,1,0)}}{\Omega_0^{(0,0,0)}}\right\|_2, \tag{46b}$$

$$\mathrm{Re}_w = w_N/n_C = \frac{6}{n_C}\left\|\frac{\Omega_2^{(0,0,1)}}{\Omega_0^{(0,0,0)}}\right\|_2. \tag{46c}$$

In a statistically isotropic particle distribution, the magnitudes of artificial cell Reynolds number and normal diffusivity in *x*, *y*, and *z* directions are nearly the same and are independent of particle

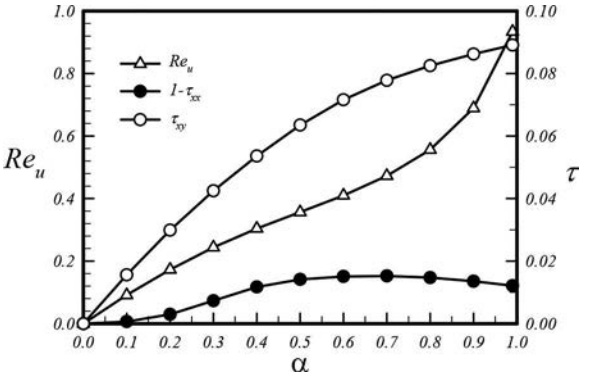

Figure 17. Artificial cell Reynolds number of PS and diffusivity of IPS.

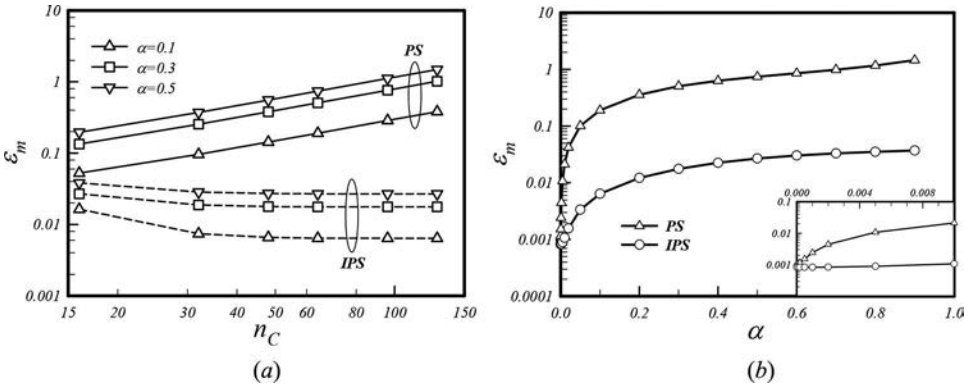

Figure 18. Error of the difference Laplacian operator. (*a*) Effect of the particle spacing (α = 0.3), (*b*) effect of the grid irregularity ($n_C = 64$).

number density. Meanwhile, the numerically induced shear diffusivity accounts for mainly the solution inaccuracy of IPS as compared with its normal part. Since these numerically induced quantities are not influenced by the particle spacing in a sufficiently dense grid environment, the predicted error

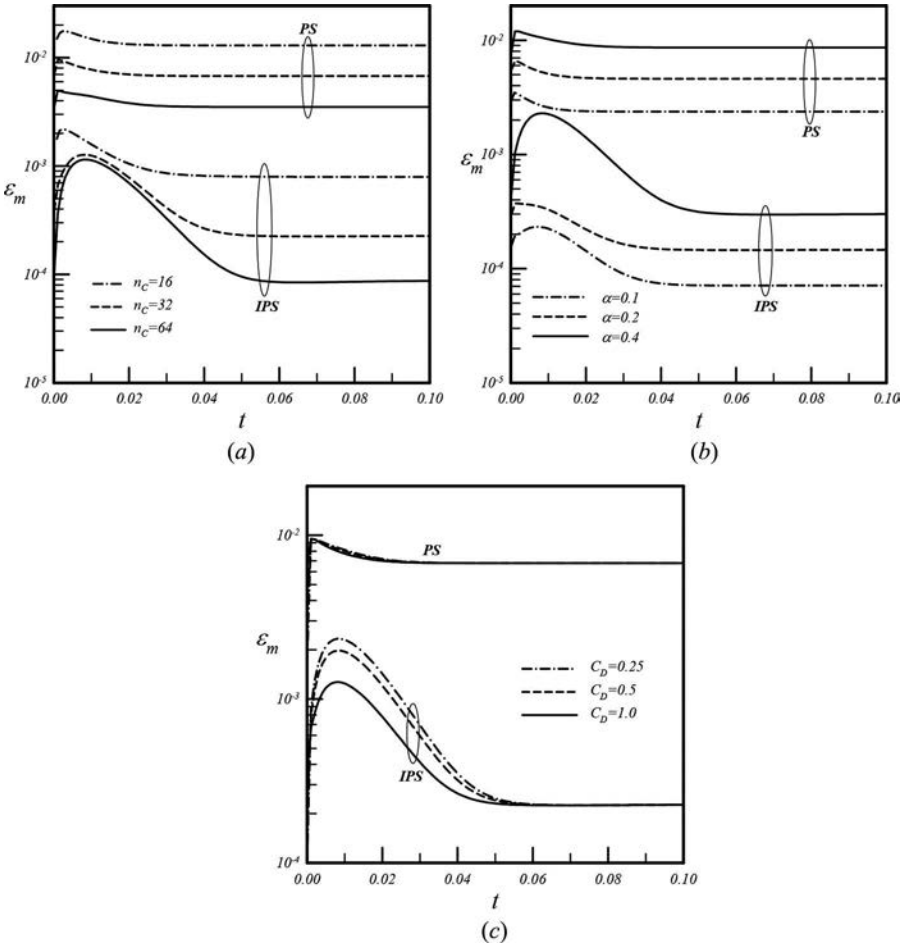

Figure 19. Evolution of the solution error. (*a*) Effect of the particle spacing, (*b*) effect of the grid irregularity, and (*c*) effect of the time step.

will then be attributed to the grid irregularity factor. Figure 17 plots the parameters: Re_u, $1-\tau_{xx}$, and τ_{xy} in terms of the grid irregularity with $n_C = 64$. It clearly shows that the numerical diffusivity of IPS is dominated by its shear component instead of the normal part.

The following solution distribution and its resulting exact Laplacian are considered to evaluate the difference operator:

$$\phi(x,y,z) = \sin(2\pi x)\sin(2\pi y)\sin(2\pi z), \tag{47a}$$

$$\nabla^2\phi_{\mathrm{ex}}(x,y,z) = -3(2\pi)^2\sin(2\pi x)\sin(2\pi y)\sin(2\pi z). \tag{47b}$$

Comparison of difference Laplacian operator errors is conducted and the results are exhibited in Figure 18(*a*) and 18(*b*) to signify the effects of particle spacing and grid irregularity, respectively. These results are attributed to the artificial velocity and numerically induced diffusivity as reported in Figures 16 and 17. As in the one- and two-dimensional cases, the IPS scheme can improve the estimated Laplacian operator and it is less sensitive to the grid irregularity.

The pure diffusion problem is considered by solving the following equation:

$$\frac{\partial\phi}{\partial t} = \frac{\partial^2\phi}{\partial x^2} + \frac{\partial^2\phi}{\partial y^2} + \frac{\partial^2\phi}{\partial z^2}. \tag{48a}$$

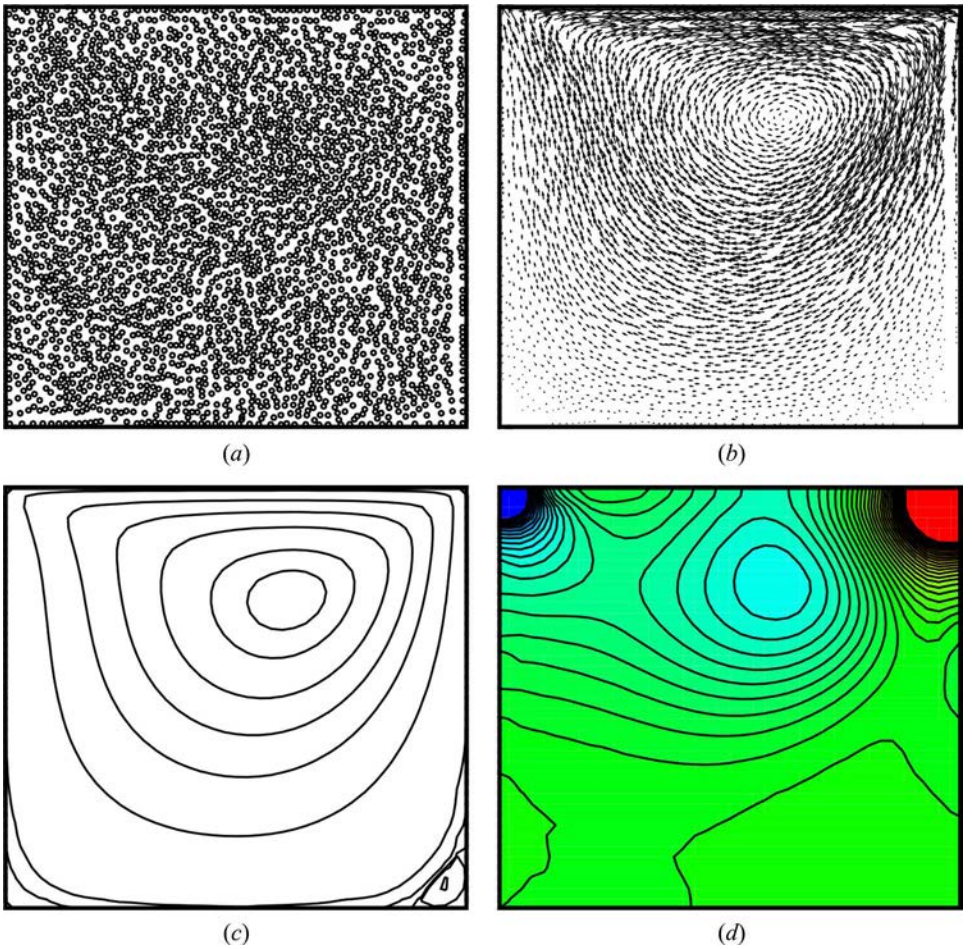

Figure 20. Results of the cavity flow computed with IPS at $t = 20$. (*a*) Particle distribution, (*b*) velocity vector, (*c*) streamlines, and (*d*) mean pressure contours.

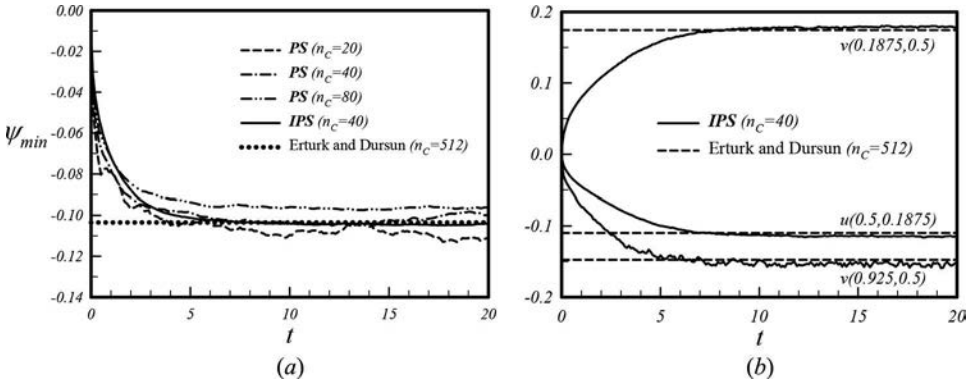

Figure 21. Results of the cavity flow with the IPS. (*a*) Evolution of the circulation flow rate and (*b*) evolution of the velocity quantities.

whereby the exact solution is available:

$$\phi_{ex}(x,y,z) = \beta e^{-12\gamma^2\pi^2 t}\sin(2\pi\gamma x)\sin(2\pi\gamma y)\sin(2\pi\gamma z) + 4x(x-1) - 4y(y-1) + (x-1/2)(y-1/2)(z-1/2).$$

As in the one-dimensional case, the simple Euler forward scheme is adopted to solve this problem with the time step assigned as:

$$\Delta t = C_D \frac{\Omega_0^{(0,0,0)}}{6\Omega_2^{(0,0,0)}}. \tag{48c}$$

It is worth noting that a monotone solution can be obtained with $C_D \leq 1$ for PS. Calculations are performed using the following parameters:

$$n_C = 32, \quad \alpha = 0.3, \quad \beta = 1.0, \quad \gamma = 1.0, \quad \text{and} \quad C_D = 1.0. \tag{48d}$$

The predicted errors are plotted in Figure 19(*a*)–19(*c*) to investigate the effects of n_C, α, and C_D, respectively. As clearly shown in these figures, the IPS increases the solution accuracy for all cases. It is also shown that the adoption of a denser particle spacing may not significantly increase the solution accuracy. Solution accuracy will be deteriorated by grid irregularity. The resulting solution is insensitive to the adopted time step for PS. However, solution accuracy will be increased with the increasing time step for IPS in this circumstance.

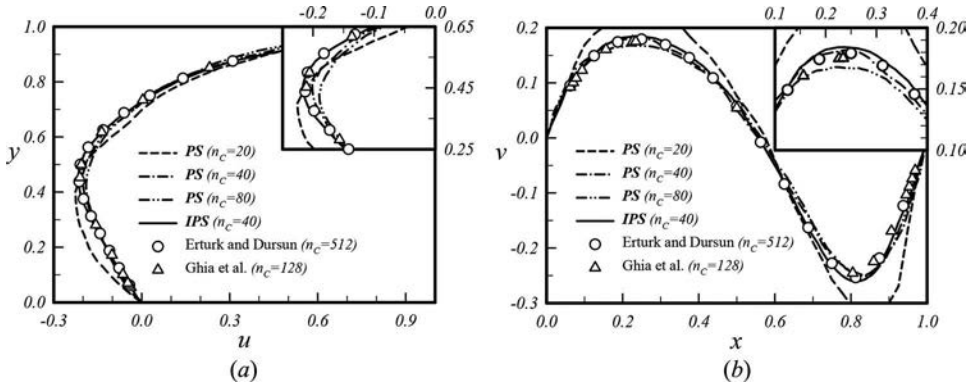

Figure 22. Comparison of the velocity profiles. (*a*) Horizontal velocity component and (*b*) vertical velocity component.

4.4. Flow problems

Finally, the proposed scheme is used to solve the lid-driven cavity and backward-facing step flow problems. Although these flow domains are geometrically simple, many complicated flow structures such as the shear, impingement, and recirculation flow can be recognized. These cases are well recognized as benchmark for validating a numerical scheme. These problems are solved by our recently developed moving particle method (MPPM), where all the pressure-related operators are resolved with the aid of a stationary inserted pressure mesh [15]. Only the flow diffusion term is evaluated at the scattered particles. For the detailed working equations, numerical schemes, and

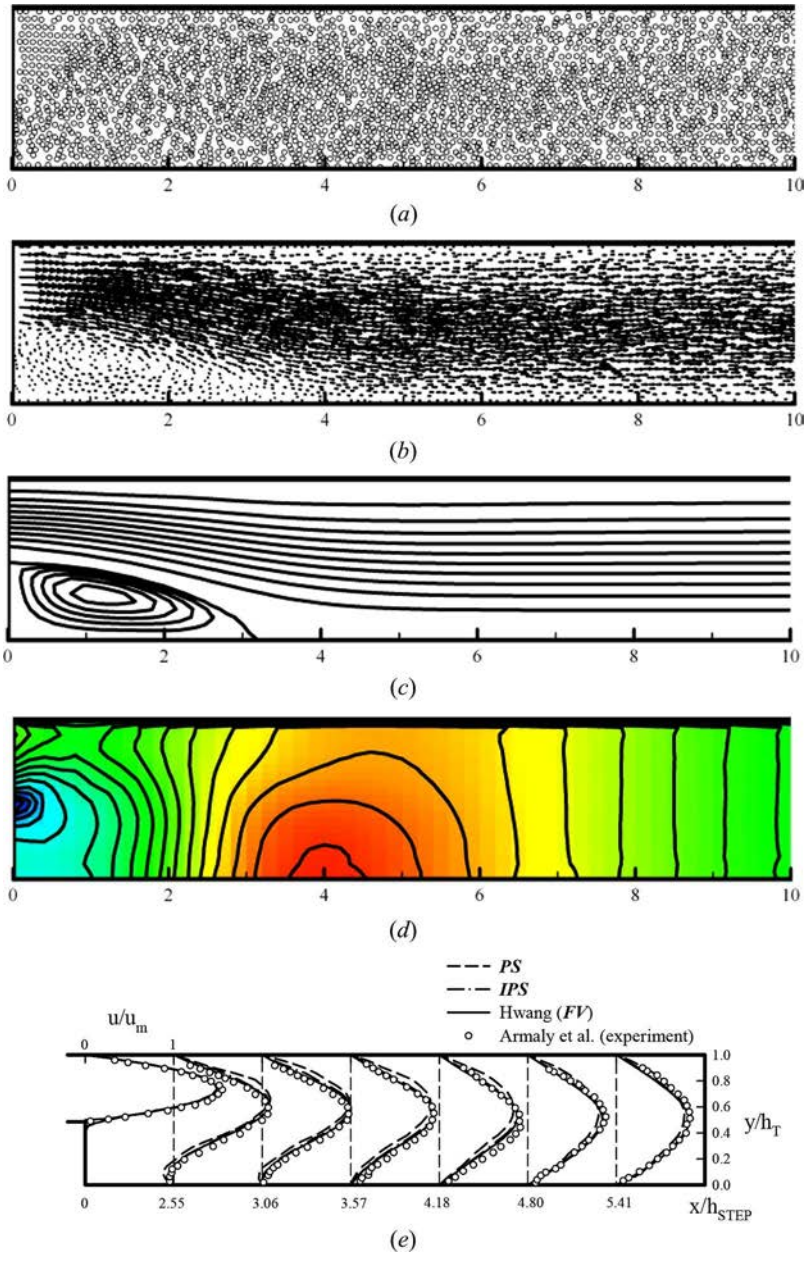

Figure 23. Results of the backward-facing step flow problem. (*a*) Particle distribution, (*b*) velocity vector, (*c*) streamlines, (*d*) mean pressure contours, and (*e*) comparison of the horizontal velocity profiles.

computational results, one can refer to [15,19, 21–23]. In the present study, the diffusion operator will be tested with the proposed IPS scheme.

Figure 20(*a*)–20(*d*) illustrate the resulting particle distribution, velocity vector, streamlines, and mean pressure contours calculated by IPS at $t = 20$ for the case of cavity flow with the Reynolds number Re $= 100$ and the initial particle spacing $\Delta x = \Delta y = 0.025$ or $n_C = 40$, respectively. The particle distribution is quite uniform and a large rotational flow structure can indeed be observed. Figure 21(*a*) compares the time evolution of the recirculation flow rates. The reference values were obtained from Erturk and Dursum [24], whereby they have solved the lid-driven cavity flow problem on a relatively dense 512×512 grid using the stream function–vorticity formulation. For comparison purpose, the results predicted by the original PS scheme with $n_C = 20$, 40 and 80 are included as well. Indeed, the predicted value by PS deviates from the reference one with an even refined particle spacing. Such a deviation is attributed to the inaccurate representation of Laplacian operator. More accurate and smoother results can be obtained with IPS. Figure 21(*b*) depicts the time evolution of velocity quantities at some typical locations. Reference solutions obtained by Erturk and Dursum [24] are also plotted for the sake of comparison. It is found that all the computed velocity quantities are in good agreement with the reference one. Comparison of velocity profiles along the cross sections in the cavity flow problem is performed in Figure 22(*a*) and 22(*b*) for the horizontal and vertical components, respectively. Results obtained by Ghia et al. [25] as well as by Erturk and Dursum [24] are also plotted in these figures. These results indicate that IPS is more accurate than PS whose accuracy cannot be improved by refining the particle spacing.

In the backward-facing step flow problem, we consider the one with expansion ratio of $(h_{\mathrm{IN}} + h_{\mathrm{STEP}})/h_{\mathrm{IN}} = 1.942$, where h_{IN} and h_{STEP} denote the inlet and step heights, respectively. Nonuniform particle distribution obtained from the embedded pressure mesh is used to reduce the computational effort. Detailed descriptions on the computational parameters can be found in [15, 19, 21, 22]. The resulting particle distribution, velocity vector, streamlines, and mean pressure contours calculated by IPS at $t = 100$ are, respectively, depicted in Figure 23(*a*)–23(*d*) for the case of Reynolds number Re $= 100$. This Reynolds number is defined by the inlet mean velocity, fluid viscosity, and inlet hydraulic diameter. As shown in these figures, quite reasonable results can be acquired with the present formulation. Figure 23 (*e*) compares the predicted result with the experimental data of Armaly et al. [26] and the high-resolution finite volume (FV) results in [27]. It is clearly demonstrated that the accuracy of the proposed IPS scheme is on par with that of the FV method, and these solutions come closer to the experimental data as compared to that of the original PS scheme.

5. Conclusion

Within the context of Lagrangian moving particle method, approximation of convection terms can be avoided and the numerical stability problem in a grid-based method can be resolved. However, diffusion term must be approximated with special care in a randomly distributed particle cloud. Because of the lack of a topology connection among particles, the differential operator may not be accurately approximated. Conventional particle smoothing procedure used to approximate the diffusion operator is derived based on the uniformly distributed particle cloud which may not be found in practical flow situations. From the simple analysis using the Taylor series expansion, the PS scheme suffers from a severe problem which is closely related to the numerically generated artificial convection term that has found to be overwhelmingly deteriorate the solution accuracy. Therefore, a simple modification is proposed in the present work to eliminate this artificial convection term. One-, two-, and three-dimensional problems have been analyzed and the proposed IPS scheme is more accurate while simulating the fluid flow conduction and two practical flow problems in the context of moving particle methods.

References

[1] L. B. Lucy, Numerical Approach to the Testing of the Fission Hypothesis, *Astronomical J.*, vol. 82, pp. 1013–1024, 1977.

[2] R. A. Gingold, J. J. Monaghan, Smoothed Particle Hydrodynamics—Theory and Application to Non-spherical Stars, *Mon. Not. R. Astron. Soc.*, vol. 118, pp. 357–89, 1977.
[3] J. J. Monaghan, Simulating Free Surface Flows with SPH, *J. Comput. Phys.*, vol. 110, pp. 399–406, 1994.
[4] H. Gotoh, T. Sakai, Lagrangian Simulation of Breaking Waves using Particle Method, *Coastal Eng. J.*, vol. 41, pp. 303–326, 1999.
[5] S. Li, W. K. Liu, Meshfree and Particle Methods and their Applications, *ASME J. Appl. Mech. Rev.*, vol. 55, pp. 1–34, 2002.
[6] C. S. Chew, K. S. Yeo, C. Shu, A Generalized Finite-difference (GFD) ALE Scheme for Incompressible Flows Around Moving Solid Bodies on Hybrid Meshfree-Cartesian Grids, *J. Comput. Phys.*, vol. 218, pp. 510–548, 2006.
[7] A. J. Chorin, Numerical Study of Slightly Viscous Flow, *J. Fluid Mech.*, vol. 57, pp. 785–796, 1973.
[8] J. J. Monaghan, Particle Methods for Hydrodynamics, *Comp. Phys. Rep.* vol. 3, pp. 71–124, 1985.
[9] J. U. Brackbill, Particle Methods, *Int. J. Numer. Meth. Fluids*, vol. 47, pp. 693–705, 2005.
[10] G. R. Liu, M. B. Liu, *Smoothed Particle Hydrodynamics*, World Scientific Publishing Co., Singapore, 2003.
[11] S. Koshizuka, Y. Oka, Moving-particle Semi-implicit Method for Fragmentation of Incompressible Fluid, *Nucl. Sci. Eng.*, vol. 123, pp. 421–434, 1996.
[12] C. L. Huang, T. W. H. Sheu, T. Ishikawa, T. Yamaguchi, Development of a Particle Interaction Kernel for Convection–Diffusion Scalar Transport Equation, *Numer. Heat Transfer B*, vol. 60, pp. 96–115, 2011.
[13] S. J. Cumming, M. Rudman, An SPH Projection Method, *J. Comput. Phys.* vol. 152, pp. 584–607, 1999.
[14] E.-S. Lee, C. Mouline, R. Xu, D. Violeau, D. Laurence, P. Stanley, Comparisons of Weakly Compressible and Truly Incompressible Algorithm for the SPH Mesh Free Particle Method, *J. Comput. Phys.*, vol. 227, pp. 8417–8436, 2008.
[15] Y.-H. Hwang, A Moving Particle Method with Embedded Pressure Mesh (MPPM) for Incompressible Flow Calculations, *Numer. Heat Transfer B*, vol. 60, pp. 370–398, 2011.
[16] R. Kech, D. Hietel, A Projection Technique for Incompressible Flow in the Meshless Finite Volume Particle Method, *Adv. Comput. Math.*, vol. 23, pp. 143–169, 2005.
[17] A. K. Chaniotis, D. Poulikakos, P. Koumoutsakos, Re-meshed Smoothed Particle Hydrodynamics for the Simulation of Viscous and Heat Conducting Flows, *J. Comput. Phys.*, vol. 182, pp. 67–90, 2002.
[18] B. Naryoles, G. Touzot, P. Villon, Generalizing the Finite Element Method: Diffuse Approximation and Diffuse Elements, *Comput. Mech.*, vol. 10, pp. 307–318, 1992.
[19] Y. -H. Hwang, Assessment of Diffusion Operators in a Novel Moving Particle Method, *Numer. Heat Transfer B*, vol. 61, pp. 329–368, 2012.
[20] S. Zhang, K. Morita, K. Fukuda, N. Shirakawa, An Improved MPS Method for Numerical Simulations of Convective Heat Transfer Problems, *Int. J. Numer. Meth. Fluids*, vol. 51, pp. 31–47, 2006.
[21] Y. -H. Hwang, Smoothing Difference Scheme in a Moving Particle Method, *Numer. Heat Transfer B*, vol. 60, pp. 203–234, 2011.
[22] Y. -H. Hwang, Implementation of Point-implicit Diffusion Operator in a Moving Particle Method (MPPM), *Numer. Heat Transfer B Fund.*, vol. 62, pp. 315–340, 2012.
[23] Y. -H. Hwang, H. -S. Huang, Simulations of the Incompressible Axisymmetric Flow with a Moving Particle Method (MPPM), *Numer. Heat Transfer B Fund.*, vol. 63, pp. 139–166, 2013.
[24] E. Erturk, B. Dursum, Numerical Solutions of 2-D Steady Incompressible in a Driven Skewed Cavity, *ZAMM-J. Appl. Math. Mech.*, vol. 87, pp. 377–392, 2007.
[25] U. Ghia, K. N. Ghia, C. T. Shin, High-resolutions for Incompressible Flow using the Navier-Stokes Equations and a Multigrid Method, *J. Comput. Phys.*, vol. 48, pp. 387–411, 1982.
[26] B. F. Armaly, F. Durst, J. C. F. Pereira, B. Schoung, Experimental and Theoretical Investigation of Backward-facing Step Flow. *J. Fluid Mech.*, vol. 127, pp. 473–496, 1983.
[27] Y. -H. Hwang, Development of a Compact and Accurate Discretization for Incompressible Navier-Stokes Equations Based on an Equation-solving Solution Gradient, Part III: Fluid Flow Simulations on Staggered Polygonal Grids, *Numer. Heat Transfer B*, vol. 58, pp. 193–215, 2010.